applied sciences

MDPI

Article

A Mobile Robot with Omnidirectional Tracks—Design and Experimental Research

Mateusz Fiedeń * and Jacek Bałchanowski

Faculty of Mechanical Engineering, Wroclaw University of Science and Technology, Wybrzeże, Wyspiańskiego 27, 50-370 Wroclaw, Poland; jacek.balchanowski@pwr.edu.pl
* Correspondence: mateusz.fieden@pwr.edu.pl

Abstract: This article deals with the design and testing of mobile robots equipped with drive systems based on omnidirectional tracks. These are new mobile systems that combine the advantages of a typical track drive with the advantages of systems equipped with omnidirectional Mecanum wheels. The omnidirectional tracks allow the robot to move in any direction without having to change the orientation of its body. The mobile robot market (automated construction machinery, mobile handle robots, mobile platforms, etc.) constantly calls for improvements in the manoeuvrability of vehicles. Omnidirectional drive technology can meet such requirements. The main aim of the work is to create a mobile robot that is capable of omnidirectional movement over different terrains, and also to conduct an experimental study of the robot's operation. The paper presents the construction and principles of operation of a small robot equipped with omnidirectional tracks. The robot's construction and control system, and also a prototype made with FDM technology, are described. The trajectory parameters of the robot's operation along the main and transverse axes were measured on a test stand equipped with a vision-based measurement system. The results of the experimental research became the basis for the development and experimental verification of a static method of correcting deviations in movement trajectory.

Keywords: omnivehicle; omnitracks; Mecanum rollers; FDM

check for updates

Citation: Fiedeń, M.; Bałchanowski, J. A Mobile Robot with Omnidirectional Tracks—Design and Experimental Research. *Appl. Sci.* **2021**, *11*, 11778. https://doi.org/10.3390/app112411778

Academic Editor: António Paulo Moreira

Received: 18 November 2021
Accepted: 7 December 2021
Published: 11 December 2021

Publisher's Note: MDPI stays neutral with regard to jurisdictional claims in published maps and institutional affiliations.

Copyright: © 2021 by the authors. Licensee MDPI, Basel, Switzerland. This article is an open access article distributed under the terms and conditions of the Creative Commons Attribution (CC BY) license (https://creativecommons.org/licenses/by/4.0/).

1. Introduction

In 2018, the world mobile robot market was worth USD 19 billion [1]. On the basis of the latest forecast, it is estimated that by 2023 its value will have nearly tripled. These robots have already moved from closed research centres and innovation fairs to the reality of everyday life. Autonomous transport vehicles used for supplies in storage facilities, autonomous mowers in house gardens, smart vacuum cleaners in homes, teleoperated robots, or bomb disposal robots are not only becoming a common element in company equipment, but also a commodity purchased by the average consumer [2,3]. Terrestrial mobile robots can be categorised using a number of criteria, and their constructed systems differ in terms of locomotion types. They can be wheeled, stepping, tracked, or ball balancing robots [4].

Wheeled robots are the most recognized, investigated and frequently used group of mobile robots. They achieve the highest speeds on flat surfaces. Their downside, however, is their poor ability to operate in difficult terrain, with some of them being vitiated by a significant turning radius [5]. Currently, research on improving their mobility in difficult terrain is being conducted. One new solution that has been proposed are hybrid wheeled–stepping robots [6–8].

At the opposite end of the robot spectrum are stepping robots, i.e., devices that are characterised by the best adaptation to overcome obstacles in terrain. Important disadvantages of their most common versions is low movement speed and complex problems related to the stepping control methodology (e.g., problems with maintaining balance

during dynamic stepping in unknown terrain) [9]. In recent years, research on improving the movement speed of stepping robots has been conducted [10,11].

Tracked robots can be classified as a compromise between wheeled and stepping robots. Tracks allow for the mobility of the robot in difficult terrain, while also helping them to maintain a satisfactory movement speed. This type of locomotion has been recognised, investigated and used to a significantly higher degree than stepping systems [12].

Ball-balancing robots, also called ballbots, are robots in which the wheelset system is a ball [13]. This locomotion type, apart from ensuring holonomic control, is a successful solution in robot locomotion that is used to demonstrate technology, and in toys or presentation robots. It is visually attractive. The ballbot group also encompasses robots with a spherical outer casing, or a casing resembling a spherical shape [14,15]. Due to such a construction, these robots can not only achieve a high speed, but can also overcome water obstacles in difficult terrain.

Mobile robotics is now at the stage of dynamic development, where it quickly adapts to novel technological solutions while maintaining some previously used ones. Various simple solutions are successfully used in modern applications. Paper [16] addresses the issues of the hybridization of animals and machines, as well as the use of robots for research on animals. Many of their functions, such as the movement of a mechanical fish, are performed by simple mechanical systems. Paper [17] describes the construction of a mobile robot, in which the stepping movements of 4 legs are produced by a single drive.

An example use of an existing and well-investigated solution can be seen in Mecanum wheel systems. They were patented in 1972 by Swedish engineer Bengt Erland Ilon [18]. The wheels, due to top free rotation rollers oriented at 45° on the wheel circumference, as well as appropriate steering, allow vehicles to move in any direction on a flat surface [19] (Figure 1). Another alternative is the use of transversal rollers oriented at 0°—although such a solution means that the implementation of an optimal wheel with a minimum gap may require an expensive manufacturing process [20]."

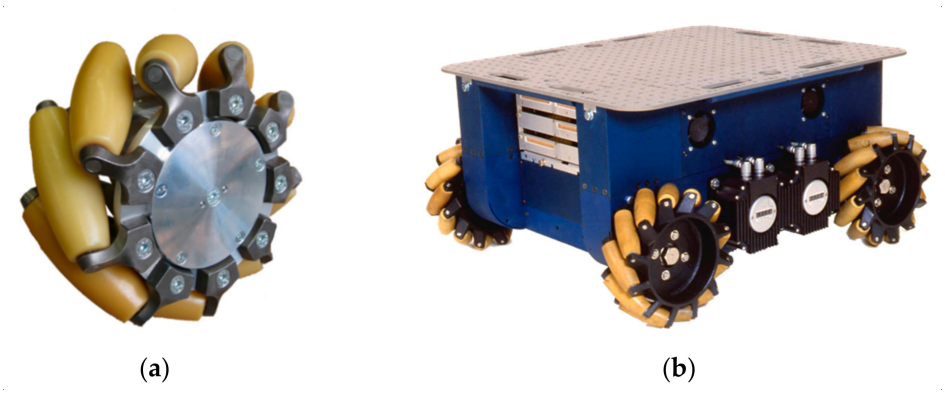

(**a**) (**b**)

Figure 1. Mecanum wheel [21] (**a**), and the URANUS mobile robot with Mecanum wheels (**b**) [22].

A four-wheeled robot with Mecanum wheels (Figure 1b), which is driven by four independent motors, can move in any direction on a plane without the necessity to rotate [19,23,24]. A robot equipped with Mecanum wheels is holonomic, so the number of controlled degrees of freedom is equal to the number of degrees of freedom that are held. This is of particular significance in the case of robots that operate in very limited spaces. Fork-lifts and transport robots with Mecanum wheels, which are therefore able to move in any direction, can be used in storage facilities and production halls in which there is a lot of equipment and a large number of storage racks in a small space.

Apart from the whole array of advantages, Mecanum wheels also have considerable disadvantages: robots and vehicles equipped with such wheels need flat, even and clean surfaces. However, there have been many investigations aimed at improving the locomotion of such systems in difficult terrain [25]. The vibration of rotating rollers, which occurs during motion, is another drawback of Mecanum wheels. The reason for this vibration is

the cyclical shifting of the load between the subsequent rollers of a wheel [26]. In most applications, the vibration will not have a significant impact on the robot's operation, however, in some specific uses it can have a significant influence on it [27]. Another potential issue is the distribution of load on the floor surface. Due to their structure, Mecanum wheels have a small wheel-surface contact area. To improve the force distribution and to prevent defects of the surface on which the robot moves, additional, surplus wheels are used in numerous applications for the purpose of reducing the impact of load on the surface. In some applications, non-driven castor wheel types are used, with additional driven Mecanum wheels being used in some others [28].

In recent years, research has been conducted on the possibility of combining Mecanum wheels with a classical drive track. Mobile robots with such a track system have all the advantages of vehicles with Mecanum wheels, but do not take on their disadvantages. They can move on uneven, dirt-covered terrain and can carry heavier loads due to the multiple number of rollers in the tracks. Systems with such a drive can be used as mobile storage robots, automated construction machines (excavators, drilling rigs) [29], inspection or rescue robots, transport platforms and bomb disposal robots. The use of multidirectional tracks in the construction of mobile robots significantly increases their maneuverability.

In 1999, in Isod's work [30], the issue of multidirectional tracked robots was discussed. Such attempts to transfer the properties of Mecanum wheels to tracked wheels were made in 2015 and are described by Zhang [31].

In 2017, a German company, IVA Johann GmbH, in cooperation with scientists from the Bremer Institut für Produktion und Logistik, presented a commercial prototype of a mobile robot equipped with multidirectional tracks [29]. In 2018, the results of simulation research conducted by Zhang [32] on a platform equipped with multidirectional tracks were published. In 2020, Fang published research results involving the construction and tests of a fork-lift equipped with multidirectional tracks, which was designed to transport loads of a maximum of 2 tons [33]. During the research, which was both experimental and numerical, it was shown that a robot with multidirectional tracks preserves its holonomic characteristic.

The paper published by Huang discussed mobility in difficult terrain [34]. During movement along the robot's main axis, multidirectional tracks preserve the robot's ability to overcome terrain obstacles, such as embankments, stairs, thresholds or curbs. In the case of transverse movement to the robot's main axis, the ability to overcome thresholds and steps was significantly reduced. Due to the ability to overcome obstacles while travelling along the main axis, the new robot will replace systems with Mecanum wheels in warehouse facilities and production halls that may have floors with uneven surfaces, thresholds and kerbs.

Simulation research results on rectilinear motion in the transverse direction of a robot with multidirectional tracks are presented in [33]. It was demonstrated that the robot's motion trajectory becomes curved during such motion, which was also confirmed by the experimental research discussed in [32]. Deviations from the rectilinear path depend on the robot's mass, and such deviations increase with a decrease in system mass. An article written by Huang [34] also discusses research on the transverse motion of a robot on a smooth and slippery surface and includes the problems resulting therefrom.

Primarily robots with longitudinally symmetric non-overlapping tracks were investigated in the publications referred to above, and only in one case were robots with symmetric and partly overlapping tracks scrutinized. However, the publications do not discuss issues related to the applications of non-symmetric tracks, nor do they discuss other track systems. Research on the influence of load on driving properties has been conducted for robots with a mass of a maximum of 5 tons. The issue of vibration during the locomotion of robots with multidirectional tracks was not discussed. No attempt to compensate for deviations of direction during locomotion was made.

In this paper is developed a new mobile robot with a drive system that uses multidirectional tracks. The research encompasses the ability of a prototype to perform basic manoeuvres, i.e., motion along the main and transverse robot axes. A static method of im-

proving motion parameters by correcting control parameters was developed and verified. The tests were conducted on a prototype made with fused deposition modelling (FDM) 3D printing technology on a test bench equipped with a vision-based measurement system.

2. Materials and Methods

2.1. Construction of a Mobile Robot with Multidirectional Tracks

A classical vehicle with a track drive system (excavator, bulldozer, tank, armoured personnel carrier, bomb disposal robot, etc.) is made of a body and two continuous track systems located symmetrically to the body (Figure 2a). A vehicle with a drive system with multidirectional tracks is equipped with four continuous track systems, which can usually be positioned in various ways with regards to the vehicle's body. The typical schemes of continuous track positions encompass tracks that are completely overlapping (Figure 2b), tracks that are partially overlapping (Figure 2c), as well as systems with non-overlapping tracks (Figure 2d).

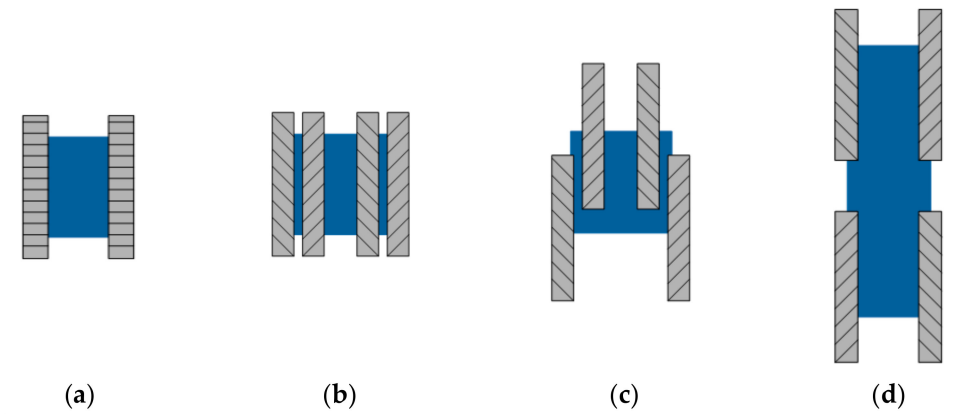

Figure 2. Schemes of track positions with two and four continuous tracks: (**a**) symmetrical system, (**b**) symmetrical system with completely overlapping tracks, (**c**) system with partially overlapping tracks, (**d**) system with non-overlapping tracks.

It was assumed that the mobile robot to be constructed would have the structure of a symmetrical system with completely overlapping tracks, i.e., it will be made of a body and four parallel track drive systems of equal length with completely overlapping tracks (Figure 2b).

During contact between the continuous track and the surface, tractive force is generated. This force is necessary for a vehicle to move. A large surface-track contact area and an appropriately adjusted track preload result in a lower unit pressure of the track when compared to the wheel. A standard, single continuous track system is made of a track located between the drive wheels, idler, road wheels and return rollers (Figure 3a). In some track vehicles (e.g., excavators), there are solutions in which the drive wheels and idlers also take the load-carrying capacity (Figure 3b). This type of powertrain was also selected for the designed mobile robot. However, due to the large radius of the drive wheels and idlers in relation to their spacing, no extra road wheels were used (Figure 3c).

Tracks in the continuous track system are composed of a closed sequence of several dozen links that are connected to one another with rotating pairs. In the case of multidirectional tracks, each link is equipped with an additional rotating roller positioned at angle γ (usually $30^\circ < \gamma < 60^\circ$) to the link axis. The view of a single link with length a, width b, and height h, and also a cylindrical roller with radius $r_{r,}$, is presented in Figure 4.

The designed mobile robot is equipped with four independent continuous track systems with multidirectional tracks that have only drive wheels and idlers. It is a four-degrees-of-freedom system. The drive is transferred from the rotating drives to the drive wheels using belts. In the middle part of the robot's body, at point R, the local x'y' coordinate system is located. The kinematic scheme of the robot is shown in Figure 5.

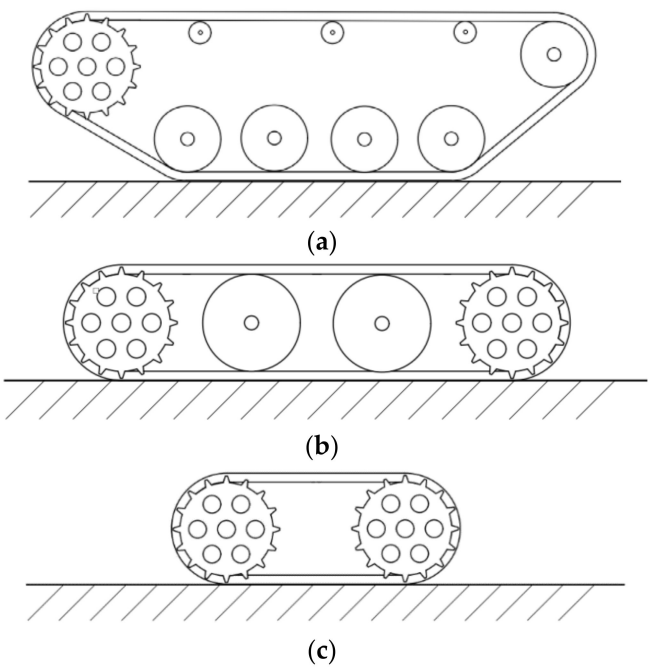

Figure 3. Continuous track system: (**a**) standard system, (**b**) system with drive road wheels, idlers and road wheels, (**c**) system with drive road wheels and idlers without road wheels.

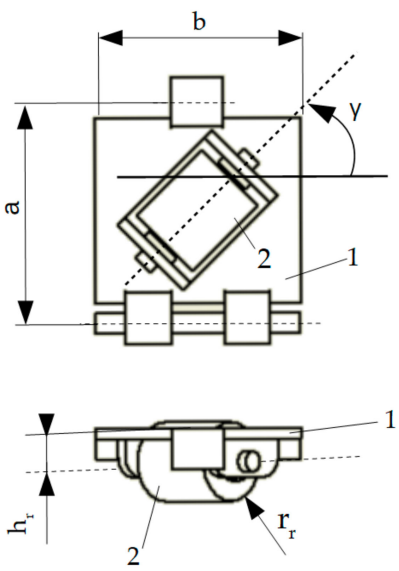

Figure 4. View of a single multidirectional track link: 1—link, 2—roller.

It was assumed that the designed robot would be used indoors (residential buildings, offices, warehouse facilities, production halls, etc.). Therefore, its dimensions must be adapted to overcome the typical obstacles seen in such places: doors, thresholds, staircases, etc. The robot should move at a maximum speed of v_R = 0.2 m/s, which is the speed considered acceptable for a robot moving in a 'human environment' [35]. This means that the maximum track speeds 1, 2, 3, 4:

$$v_R = v_1 = v_2 = v_3 = v_4 \tag{1}$$

The resulting basic dimensions are described in Table 1.

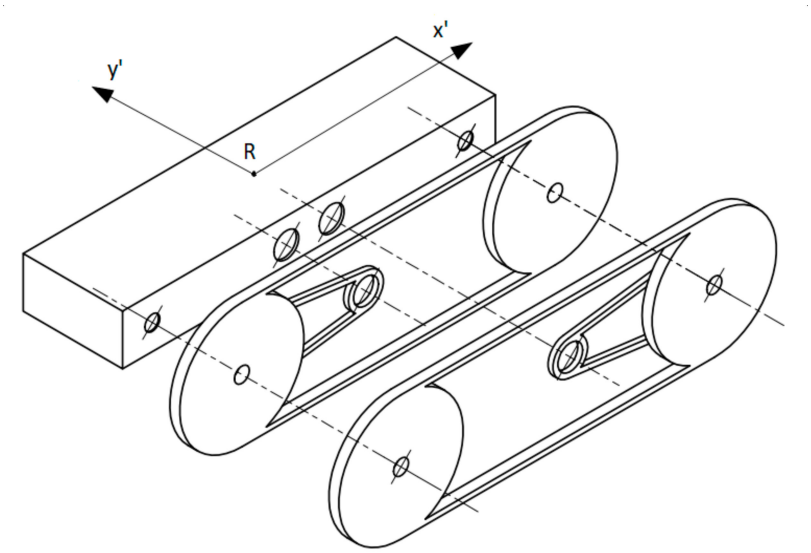

Figure 5. Kinematic scheme of the robot with a continuous track system that has multidirectional tracks.

Table 1. Dimension and construction assumptions of the mobile robot.

Dimension Name and Symbol	Value	Dimension Name and Symbol	Value
robot mass m_r	6 kg	working load u	2 kg
track link height a	45 mm	track link width b	40 mm
roller radius r_r	10 mm	distance between the axis of the roller and the plane of the track link h_r	5 mm
roller mounting angle γ	45°	distance between pairs of continuous track systems c	270 mm
distance between the continuous track systems in pair d	80 mm	distance between the axes of the driving and idler wheels e	225 mm
belt wheel radius on drive wheel r_{ks}	60 mm	belt wheel radius on motor r_s	15 mm

Figure 6 shows an overview of the developed solid model of the robot and the detailed views of the solid model of the track system.

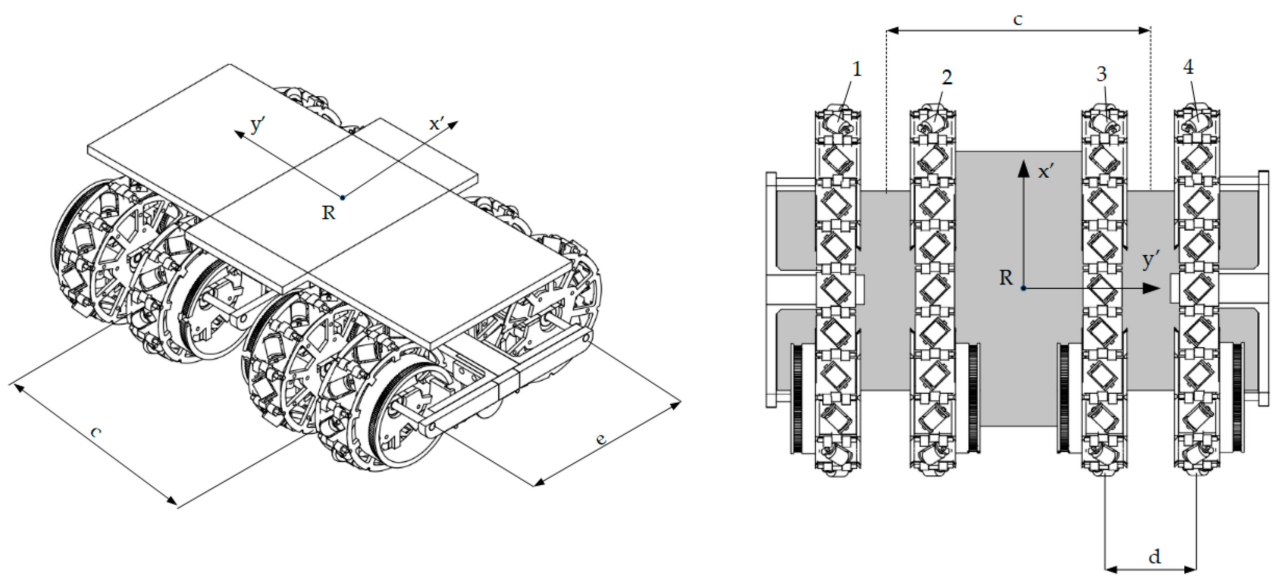

(**a**) (**b**)

Figure 6. General view (**a**) and bottom view (**b**) of the solid model of the robot with the continuous track system with multidirectional tracks.

Figure 7 shows the views of a single continuous multidirectional track with its own drive system. The continuous track system is composed of a track, an idler and a drive wheel. In each track segment there is one cylindrical rotating roller. The drives are located in the central part of the robot. The active moment is shifted to the drive wheel using transmission with a toothed belt.

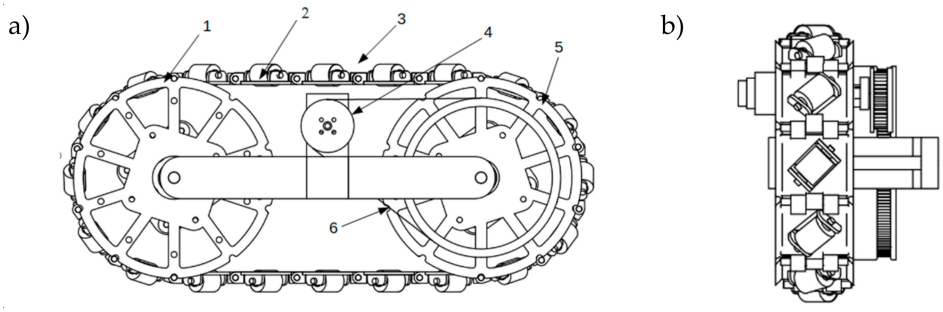

Figure 7. View of the continuous track system with multidirectional tracks: (**a**) side view and (**b**) front view (1—idler, 2—link with a rolling roller, 3—track, 4—motor pulley, 5—drive wheel, 6—toothed belt).

The track drive systems, track links, rollers and the body of the robot were made using incremental FDM technology. The material used is PET-G, which is a polymer characterised by low shrinkage and high mechanical resistance. The free rollers rotate on steel axes. There are plastic slip rings between the rollers and the mount, which is connected to the track plate. The rollers consist of a printed core, onto which the tyres are pulled. The tyres of the rollers, also made using FDM technology, are made of thermoplastic polyurethane with a Shore scale hardness of 40D. The view of the finished prototype of the mobile robot is presented in Figure 8.

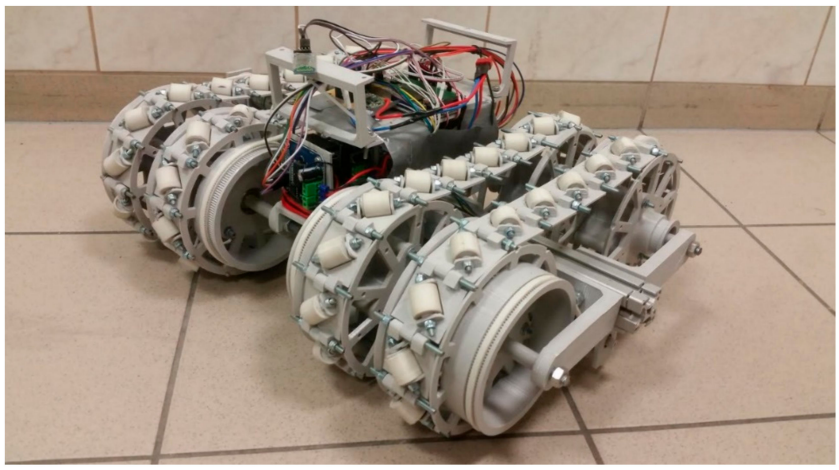

Figure 8. View of the finished robot prototype equipped with a continuous track system with multidirectional tracks.

The motor is connected to the drive wheel by a reduction pulley transmission system with a reduction ratio of $i_k = r_s/r_{ks} = 0.25$. For the assumed maximum robot motion speed v_r (Table 1), the maximum angular velocity of the motor ω_s was determined from the following equation:

$$\omega_s = \frac{v_r}{r_{ks}\, i_k} = 10.67\ rad/s \tag{2}$$

The rated active moment of motor M_s was selected using the simplified method of the experimental measurements of the robot's motion resistance in the longitudinal and transverse direction using a tensometric force sensor. The highest motion resistance was measured experimentally during motion in the direction perpendicular to the main axis,

and is expressed as the maximum force that excites motion in a set direction, which was $F_T = 13$ N. It was assumed that the motor moment M_s should be greater than:

$$M_s > \frac{r_k F_T}{4} \tag{3}$$

On the basis of the calculations made to design the prototype construction, POLOLU-2274 motors were selected with a torque of Ms = 0.57 Nm, and a nominal speed of n_s = 21.99 rad/s. Each motor is equipped with a magnetic encoder that provides 48 counts per revolution, and therefore one complete revolution of the wheel will provide 2249 pulses, with a drive wheel accuracy of $\Delta\phi_s$ = 0.0007 rad.

2.2. Control System of the Mobile Robot with Multidirectional Tracks

For the purpose of exciting the set robot motion, it is necessary to have an appropriately designed system and control algorithms. The mobile robot has four drives that independently excite the motion of each track (Figures 5 and 8). Thus, a control system is required to control the robot. The control system should have four control regulators of speed ω_{si} of motor i (i = 1, 2, 3, 4), which start the drive wheels of the continuous tracks. In the robot prototype, the speed control of the used DC motors will have the form of a pulse width modulation (PWM) signal. The general scheme of the developed robot's control system is presented in Figure 9.

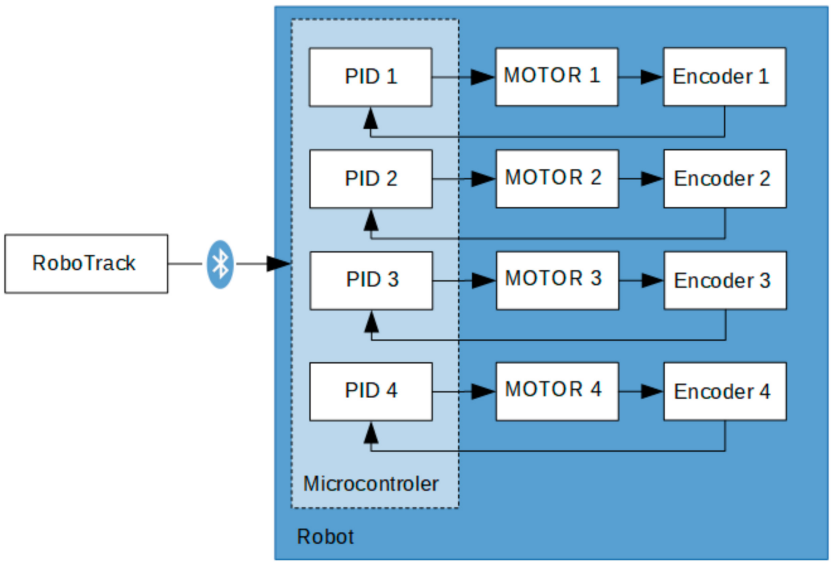

Figure 9. General block diagram of the mobile robot's control system.

Motor i, which excites the motion of the continuous track system i, is individually controlled using a PID$_i$ regulator operating in the feedback loop with a frequency of 50 Hz. The value of $v_R(t)$ is the set speed of the entire robot, the value of ω_{Ti}(t) is the value of the set speed of track motor i (i = 1, 2, 3, 4), $E_i(t)$ is the control error, $U_i(t)$ is the steering signal, $P_i(t)$ is the PWM value responsible for motor control DC, $\omega_{Mi}(t)$ is the actual motor rotational speed, $\Theta_i(t)$ is the motor rotation angle measured with an encoder, while ω_i(t) is the motor angular speed. The scheme of the speed regulator of continuous track system i is presented in Figure 10.

A RoboTrack control program was developed to control the movement of the robot. The program is run on an external PC.

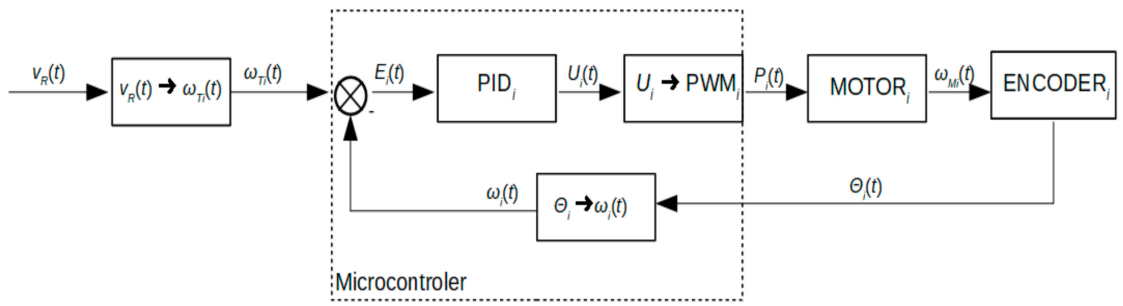

Figure 10. Scheme of the speed regulator controlling continuous track system *i* (*i* = 1, 2, 3, 4).

The programme is responsible for planning the robot's motion trajectory and for sending the set speed values $\omega_{Ti}(t)$ for particular motors *i* to the robot's control system based on speed values set by the user. RoboTrack also ensures the on-line registration of ride parameters. Communication between the external PC and the mobile robot is performed with a Bluetooth communication link

The excitation of the robot's motion along the set trajectory requires a suitable control of speeds v_1, v_2, v_3, v_4 of tracks *1, 2, 3, 4*. This paper discusses robot motion along two trajectories: a straight line μ_w at constant speed v_{Rx} along the longitudinal axis, and a straight line μ_p at constant speed v_{Ry} along the robot's transverse axis (Figure 11). In the case of motion along the longitudinal axis at speed v_{Rx}, the tracks should move at the same speeds (Figure 11):

$$v_1 = v_2 = v_3 = v_4 = v_{Rx} \tag{4}$$

while during motion along the transverse axis at speed v_{rx}, the tracks' speed takes the following values:

$$v_1 = v_3 = v_{Ry} \qquad v_2 = v_4 = -v_{Ry}. \tag{5}$$

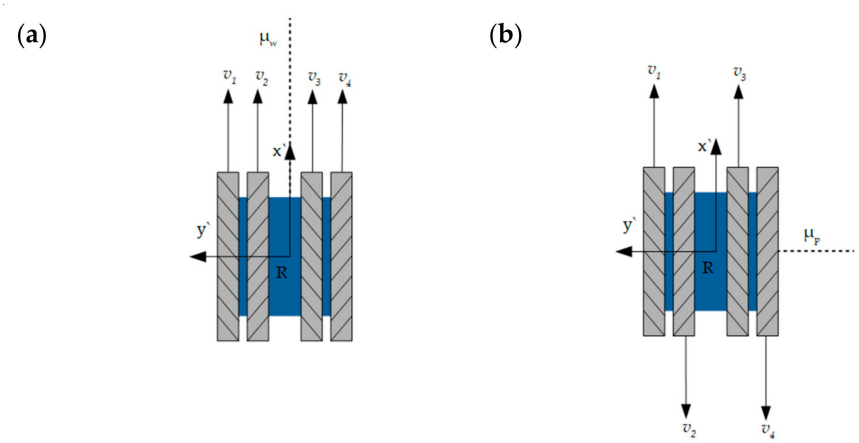

Figure 11. Scheme of the control system of continuous track system *i* (*i* = 1, 2, 3, 4) for motion along trajectory μ_w (**a**) and trajectory μ_p (**b**).

2.3. External Measurement Test Bench

The mechanical prototype proposed in this paper is not able to develop self-localization [36]. The localization of the mobile robot is determined with an external measurement test bench, the general scheme and view of which are presented in Figure 12. The vision-based measurement system was made of a camera located perpendicularly to the measured area. The ELP-USBFHD04H-MFV camera with a resolution of 1920 × 1080 px was located at the height *h* = 1.95 m with regard to the main coordinate system *xy* (Figure 12).

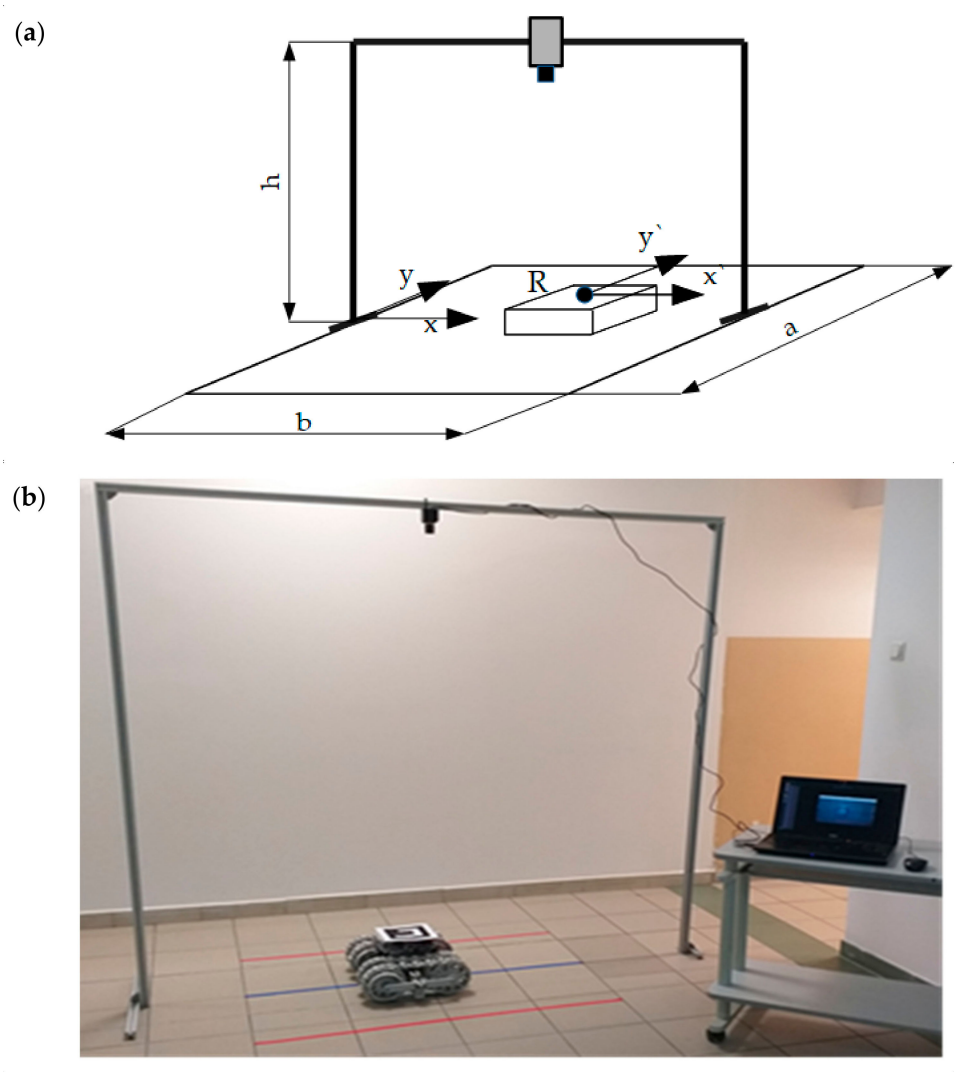

Figure 12. Robot motion test bench: (**a**) general scheme, (**b**) test bench view.

The measuring accuracy of the bench was checked using a printed calibration sheet with ArUco markers (Figure 13). The position reading error δl of the marker was less than 0.008 m and the orientation angle error $\delta\alpha$ was no more than 0.5°.

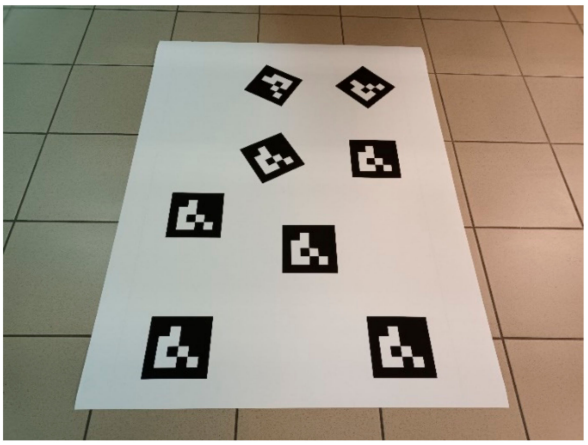

Figure 13. Calibration sheet with ArUco markers.

The vision-based system records and analyses images with a frequency of 25 Hz (frames/s). In order to allow for the detection of the robot's position in a camera image, the vision marker ArUco was placed on its top surface (Figure 14). The ArUco marker is a print on a flat tile with white and black rectangles. Owing to the precisely defined distribution of these areas, the marker can transfer its ID number, and it is therefore possible to recognize its presence in a ready image, as well as to determine its linear and angular position. For known dimensions, it is also possible to conduct a programmable estimation of its location in three-dimensional space. The middle of the marker is located in point *R* on the robot's body (Figure 14). During the measurement, the whole marker must be located in the camera vision area—this efficiently reduces the observation area to the area of the following dimensions: a = 0.75 m, b = 1.30 m.

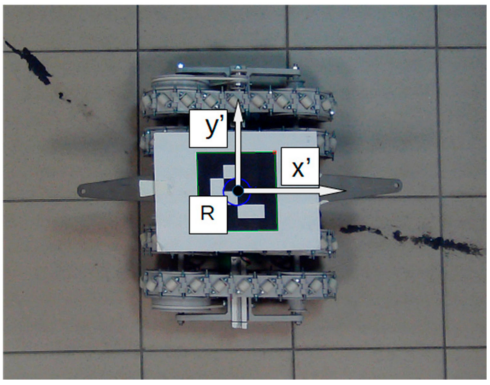

Figure 14. ArUco marker view on the robot's body.

The robot is controlled by RoboTrack software (Figure 15), which allows robot motion to be controlled and track and motor motion to be registered. The software was integrated with a VisionM module that allows the covered distance to be measured and recorded. This module is based on OpenCV libraries that are extended with OpenCV Contrib [37] modules. Its task is the online analysis of individual image frames recorded by a camera placed on the test stand. The module provides data on the angular orientation of the tracked robot, its current location and the distance covered, which are recorded in real time.

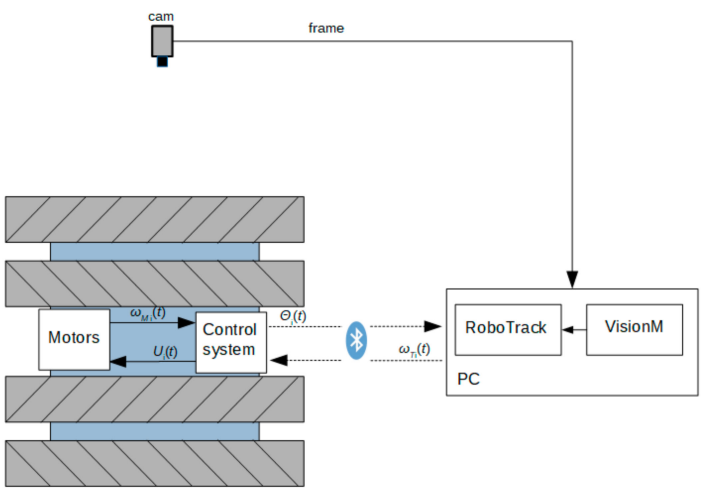

Figure 15. Data flow at the measurement test bench.

2.4. Static Correction Method of the Robot's Locomotion Direction

During the motion of the mobile robot with the continuous track system with multi-directional tracks travelling at a constant speed, the phenomenon of curved trajectories may take place [24,27]—the middle *R* of the robot's body deviates from the trajectory,

and the orientation angle α_R of the body changes. The deviations from the straight-line trajectory depend on the robot's mass, and they increase with the system's mass [27]. During movement along the transverse axis, the problems with maintaining straight line movement become even more significant when the robot moves on a slippery surface. This disadvantageous phenomenon can be prevented by the introduction of suitable corrections to the set speeds of particular continuous tracks.

For the purpose of maintaining the robot's motion along the set straight line trajectory, the fixed orientation angle α_R of the robot's body should be ensured by introducing suitable corrections of track speeds.

A difference in the orientation α_R of the body, i.e., between the real and set robot position, results from the robot's body rotation at constant angular speed ω_r. The rotation can be reduced by forcing the body to rotate in the opposite direction by making appropriate changes in track set speeds.

A simplified model of the change in the robot's body orientation and motion direction (Figure 16) was proposed, which entails the introduction of virtual tracks located between tracks 1 and 2,—marked as L_{12}, with 3 and 4 being marked as R_{34}. The speed v_k of the virtual tracks excites the corrective rotation of the body, which eliminates the change of orientation, can be determined from Equations (6) and (7). These equations take into consideration the change in the angle $\Delta\alpha_P$ of the orientation at time Δt, structural dimension c describing the distance between the pairs of continuous tracks, and an empirical adjustment factor c_f resulting from the surface type and the adhesion of the rotating rollers:

$$\omega_R = \frac{\Delta \propto_R}{\Delta t} \tag{6}$$

$$v_k = -\omega_R c_f \frac{1}{2} c \tag{7}$$

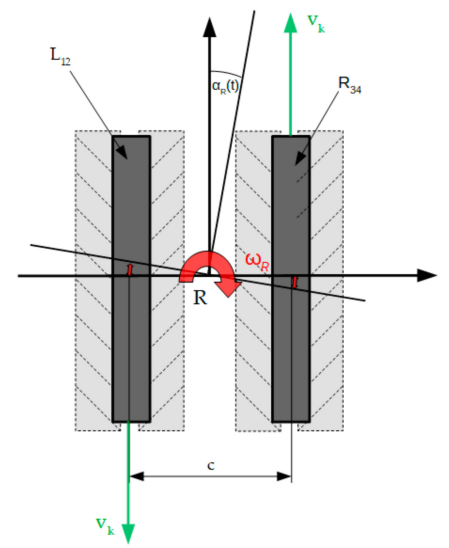

Figure 16. Illustration of the change in angular orientation α_R of the robot's body under the influence of angular speed ω_r, and also the description of this change using a method of eliminating the change in orientation by introducing corrective speeds v_k in virtual tracks R and L.

In the case of the robot's motion along the longitudinal axis, the correction of track speed involves its suitable increasing or decreasing by value v_k according to the following formula (Figure 17a):

$$v_1 = v_2 = v_{Rx} + v_k \qquad v_3 = v_4 = v_{Rx} - v_k \tag{8}$$

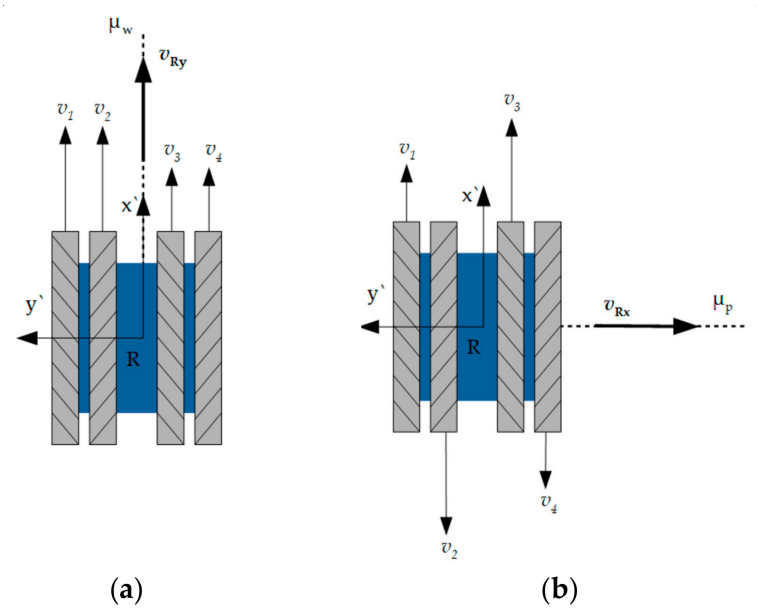

Figure 17. Illustration of track speed correction for the purpose of maintaining constant robot orientation during motion: (**a**) along the longitudinal axis along trajectory μ_w, (**b**) along the transverse axis along trajectory μ_p.

Speed correction v_k for motion along the robot's transverse axis consists of differentiating the speed on each pair of tracks according to formula (Figure 17b):

$$v_1 = -v_4 = v_{Ry} - v_k \qquad v_2 = -v_3 = v_{Ry} + v_k \tag{9}$$

2.5. Experiment Plan

A number of experimental tests of the mobile robot were carried out on the test stand in order to verify the operation of the proposed drive systems and to determine the basic kinematic properties of the movement.

The tests encompassed a number of rides on straight line trajectory μ_z located along the longitudinal and transverse axes of the robot. Various measurements of the location, the linear and angular speeds of the robot's body, the rotation angle and angular speeds of the drive wheels, and also the speed of the tracks were conducted during the rides. The research was conducted on a specially designed test bench equipped with a vision-based location measurement system. Figure 18 presents the scheme of the experiment carried out on the measurement test bench.

Ride tests were conducted at two stages. In the first part of the experiment, the set values of the linear speeds of all the tracks did not take into account the correction parameters. In the second part of the experiment, the speeds of particular drives were differentiated by the correction value, which was calculated on the basis of the proposed model of ride trajectory correction.

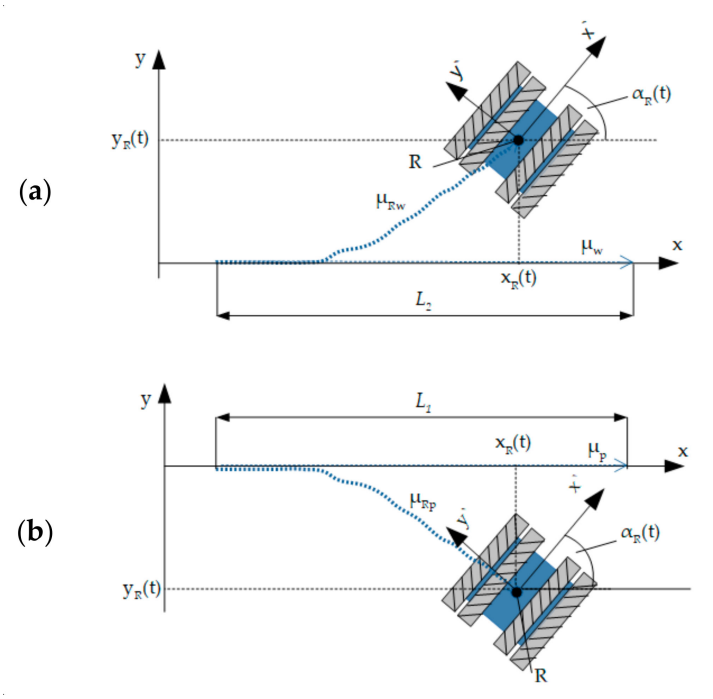

Figure 18. General scheme of the conducted tests of the robot's ride tests on a set straight line trajectory along the longitudinal axis (**a**) and along the transverse axis (**b**) of the robot (l_1, l_2—lengths of set trajectory, μ_T—set trajectory, μ_R—real trajectory, x_R(t), y_R(t)—coordinates of point R on the robot's body, α_r(t)—body coordination angle).

3. Results

The results of the measurements obtained during the investigated robot rides along the longitudinal and transverse robot axes are presented and discussed below. The tests and measurements were carried out on the designed measurement test bench (Figure 12). The length of the tested trajectory was limited by the area of the test bench. The trajectory waveforms μ_R (x_R, y_R), the dependence of change $\Delta\alpha$ on time, and the change of the coordinates x_R, y_R over time were plotted on the basis of the stationary measuring system, while the speeds of the individual tracks were determined on the basis of the angles indicated by the encoders in relation to time.

3.1. Robot Ride Tests

The tests of the robot's rides along the longitudinal axis were conducted in accordance with the scheme shown in Figure 18a. The robot moved along the planned straight-line trajectory μ_t by length L_1 = 1.2 m at the constant speed v_{Rx} = 0.12 m/s.

The scheme presented in Figure 18b shows the plan of the research on the robot's rides along the transverse axis. The robot moved along the planned straight-line trajectory μ_t by length L_2 = 1.2 m at constant speed v_{Ry} = 0.12 m/s.

During the research, the waveforms of real ride trajectories μ_R (x_R, y_R), the changes of body orientation angle $\Delta\alpha$, coordinates x_R, y_R of point R on the robot's body, and the real linear speeds v_1, v_2, v_3, v_4 of the tracks calculated on the basis of encoder indications were measured and registered. Figures 19–22 show the measurement results for rides along the longitudinal axis, while Figures 23–26 depict the measurement results of the robot's rides along the transverse axis.

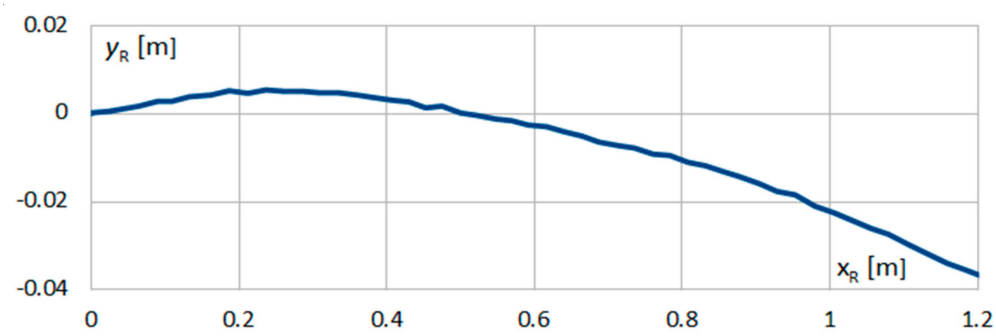

Figure 19. Trajectory μ_R (x_R, y_R) of point *R* movement on the robot's body during the ride along the longitudinal axis.

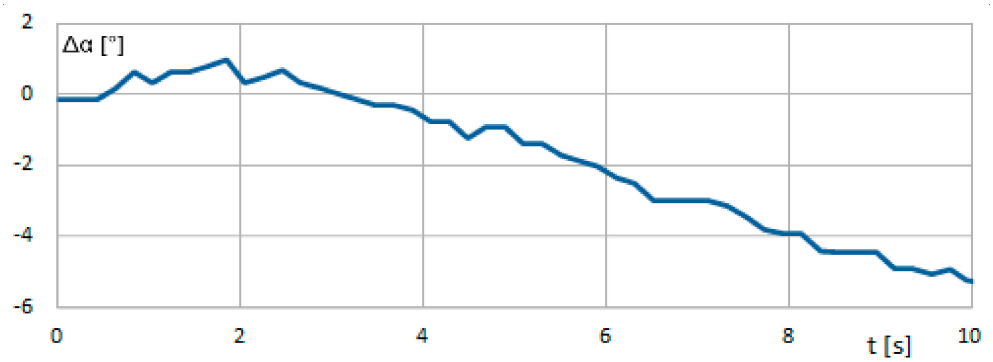

Figure 20. Waveforms of changes in angle Δα of the robot's body orientation at time *t* during the ride along the longitudinal axis.

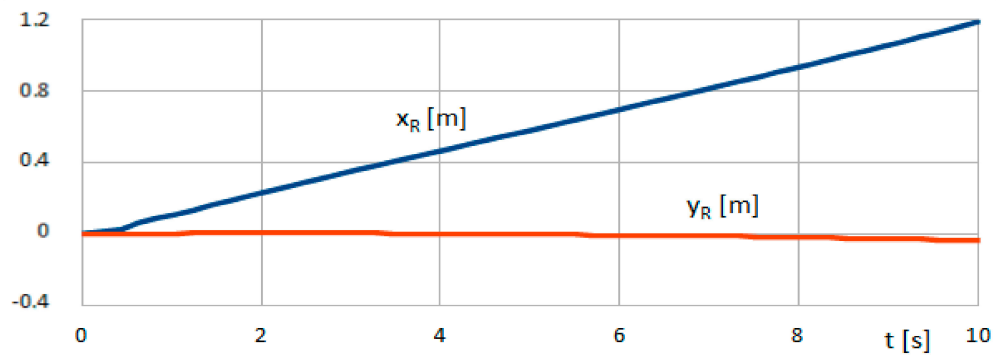

Figure 21. Plots of coordinates x_R, y_R of point *R on the robot's body* during the ride along the longitudinal axis.

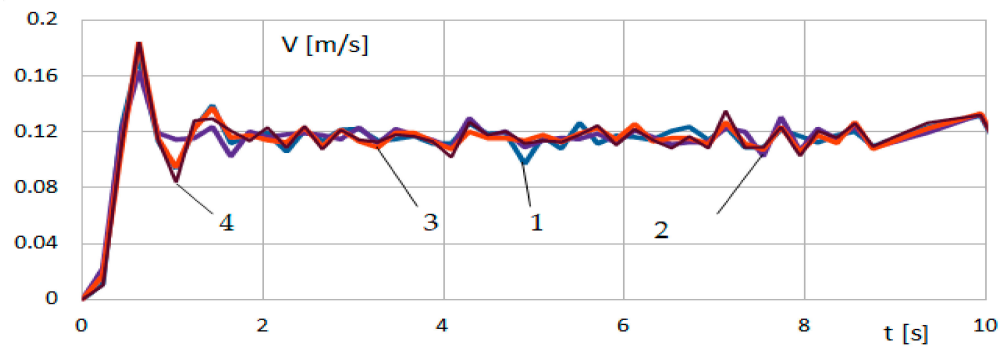

Figure 22. Waveforms of real linear speeds v_1, v_2, v_3, v_4 of tracks *1, 2, 3, 4* of the robot during the ride along the longitudinal axis.

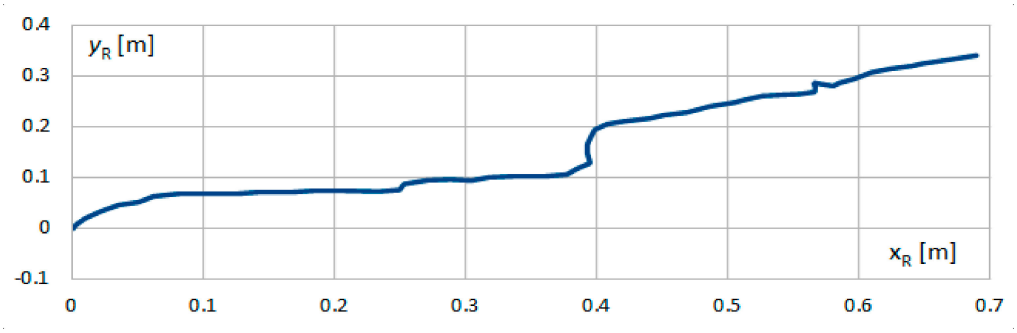

Figure 23. Trajectory μ_R (x_R, y_R) of point *R* movement on the robot's body during the ride along the transverse axis.

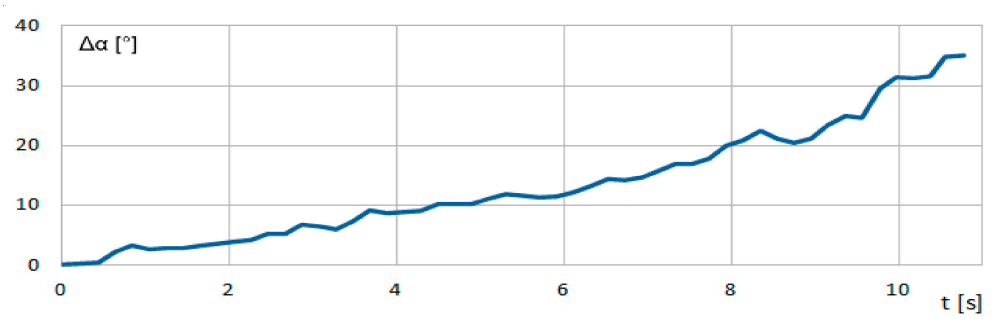

Figure 24. Waveforms of changes in angle Δα of the robot's body orientation to time *t* during the ride along the transverse axis.

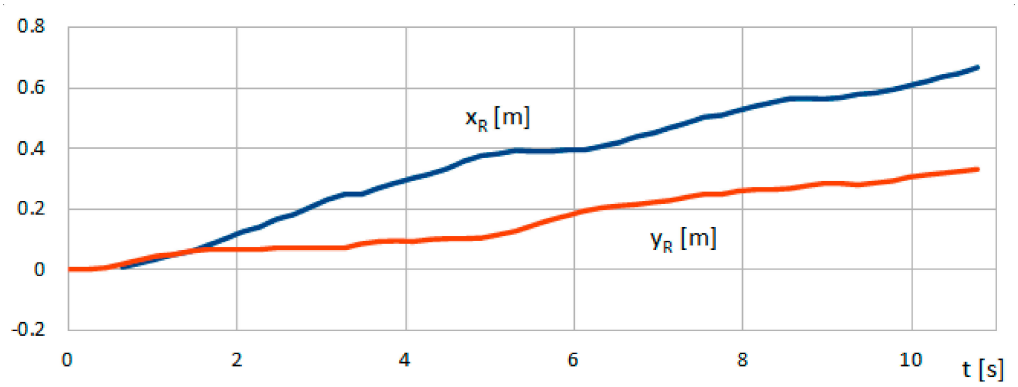

Figure 25. Plots of coordinates x_R, y_R of point *R on the robot's body* during the ride along the transverse axis.

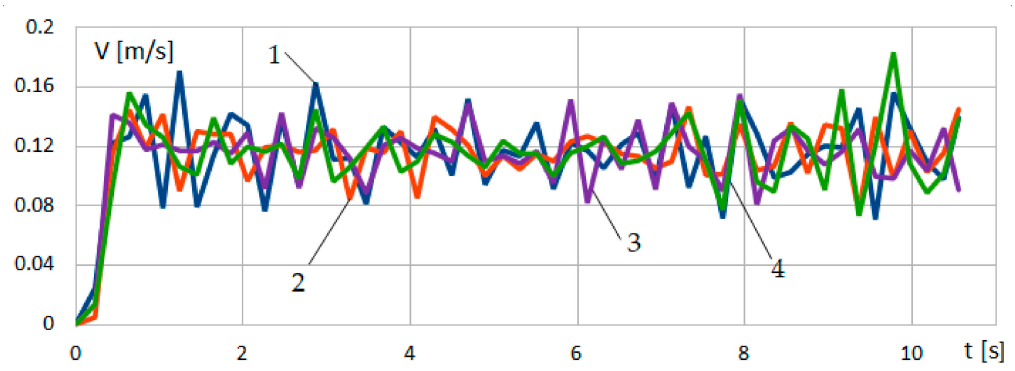

Figure 26. Waveforms of real linear speeds v_1, v_2, v_3, v_4 of tracks *1, 2, 3, 4* of the robot during the ride along the transverse axis.

The experiment showed that during the rides the real, linear speeds of tracks v_i adopted the values of the set speeds, v_{Rx} and v_{Ry}. In the case of longitudinal motion, the largest speed errors occurred at the start-up of the robot's motion. After the stabilisation of speed, the errors took significantly smaller values (Figure 22). In the case of transverse motion, the values of the track speed errors occurring at the start-up were comparable to the deviations observed during the whole ride (Figure 26). It should, therefore, be noted that no such error jump between the set and real speed in transverse motion was observed. Despite the speed jump at start-up, the maximum deviation between the real and set speed Δv_i was Δv_i =0.02 m/s for the longitudinal motion, and Δv_i =0.03 m/s for the transverse motion (Figures 22 and 26).

In both longitudinal and transverse motion, deviations from the planned trajectory were observed in the form of a curved ride and a change in the orientation of the robot's body (Figures 20 and 24). The location error of point R was determined to be $\Delta y_R = y_{RT} - y_R$. In both the longitudinal and transverse motion, the set trajectory is a straight line overlapping with the X axis of the measurement test bench coordinate system. Due to this, for both rides the theoretical location of point R in relation to the Y axis is $y_{RT} = 0$. Location deviation $\Delta y_R = y_{R.}$

In the case of the longitudinal motion, the final location error of point R was Δy_R= 0.037 m (Figure 21), while the orientation change was $\Delta\alpha$ =5° (Figure 20) at time t = 10 s.

During the transverse motion, the robot did not cover the whole planned distance (L_2 = 1.2 m), and the measurement was interrupted after it had covered the distance of 0.7 m (Figure 25) because the robot overstepped the measurement area boundary in the direction of the y axis. In the case of the transverse motion, the final orientation change was $\Delta\alpha$ = 35° (Figure 24), and the location error of point R was Δy_R= 0.36 m (Figure 25) at time t = 10.8 s.

The analysis of the waveforms of changes in the orientation angle $\Delta\alpha$ of the robot's body at time t indicated that they had a linear nature. This was confirmed by the conducted statistical analyses. The value of the Pearson linear correlation starts to be higher at 0.97 onwards for both the longitudinal and transverse motions.

3.2. Tests of Robot Rides with Consideration for the Static Correction Method of Ride Direction

The phenomenon of the change in the angle $\Delta\alpha$ of body orientation had a linear nature, and therefore the application of the static correction method set out in Section 2.5 was justified. On the basis of the planned changes of orientation angle $\Delta\alpha$ during a ride (Figures 20 and 24), the values of speed v_{kw}, corrections for the longitudinal motion, and v_{kw} for the transverse motion, were calculated using Formulas (6) and (7).

In the calculations, the adaptation factor c_f was taken into account. For the given robot's dimensions, the value of the c parameter was 0.16 m. With consideration for the type of substrate (track link rollers made of TPU filament with a hardness of 40D moving on ceramic tiles), the value of the factor was determined, empirically, to be c_f = 4.4.

The corrective speed values, obtained using Formula (7), were v_{kw} = 0.04 m/s for the longitudinal motion and v_{kp} = 0.35 m/s for the transverse motion. The corrective speed value v_{kp} = 0.35 m/s were restricted to 0.2 m/s due to the limitations of the drive and control systems of the used equipment.

For the obtained values of the corrective speed, two more tests of the robot's rides along the longitudinal and transverse axes were conducted. Figures 27–30 present the results of the measurements for the rides along the longitudinal axis, while Figures 31–34 show the results for the measurements of the robot's rides along the transverse axis.

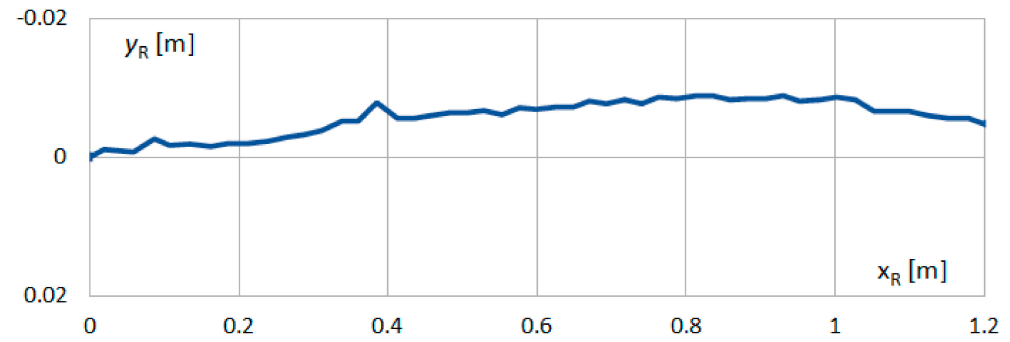

Figure 27. Trajectory μ_R (x_R, y_R) of point *R* movement on the robot's body during the ride along the longitudinal axis with ride direction correction.

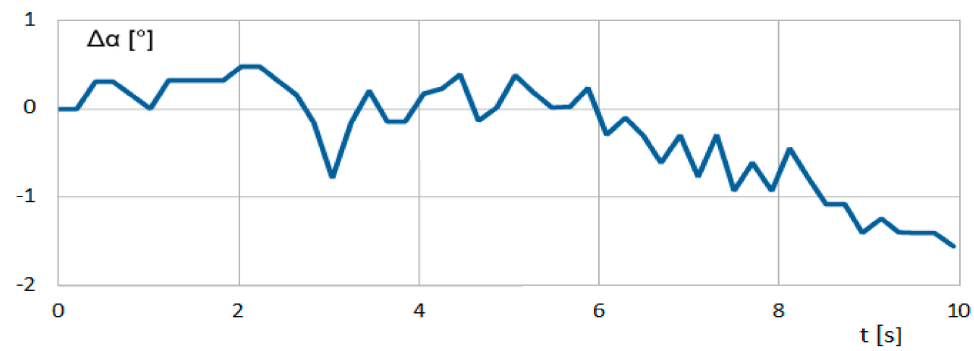

Figure 28. Waveforms of changes in angle Δα of the robot's body orientation at time *t* during the ride along the longitudinal axis with ride direction correction.

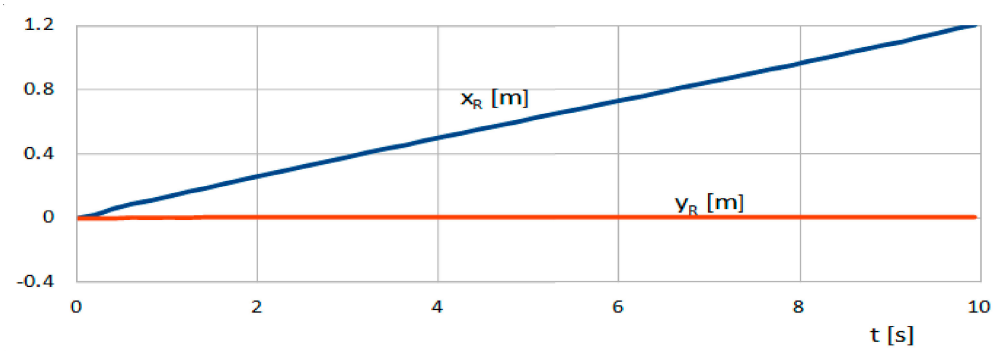

Figure 29. Plots of coordinates x_R, y_R of point *R on the robot's body* during the ride along the longitudinal axis with ride direction correction.

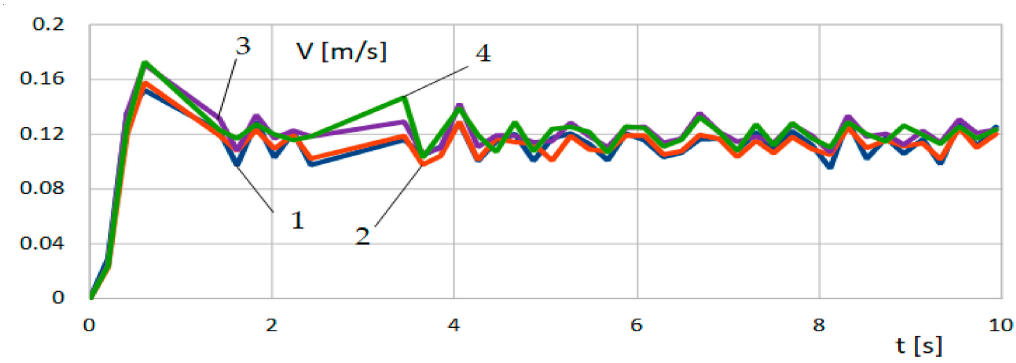

Figure 30. Waveforms of real linear speeds v_1, v_2, v_3, v_4 of tracks *1, 2, 3, 4* of the robot during the ride along the longitudinal axis with ride direction correction.

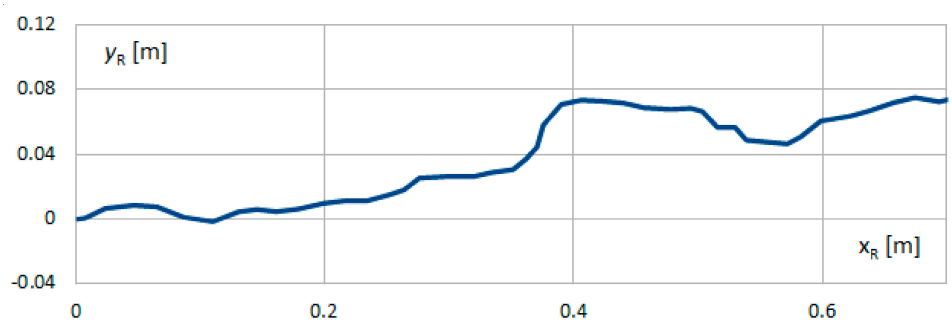

Figure 31. Trajectory μ_R (x_R, y_R) of point *R* movement on the robot's body during the ride along the transverse axis with ride direction correction.

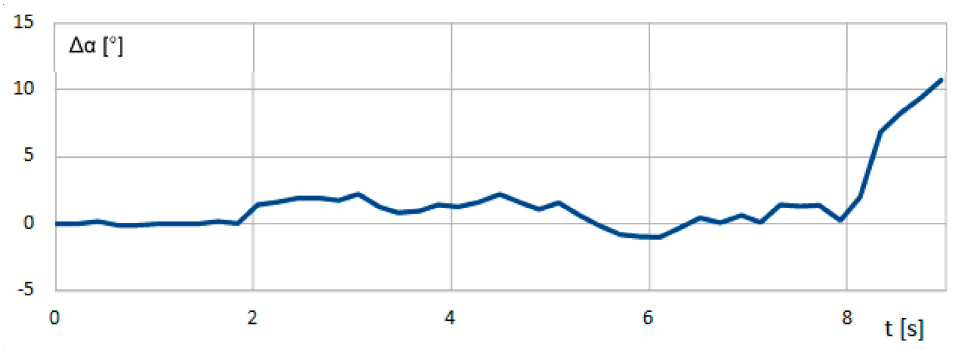

Figure 32. Waveforms of changes in angle Δα of the robot's body orientation to time *t* during the ride along the transverse axis with ride direction correction.

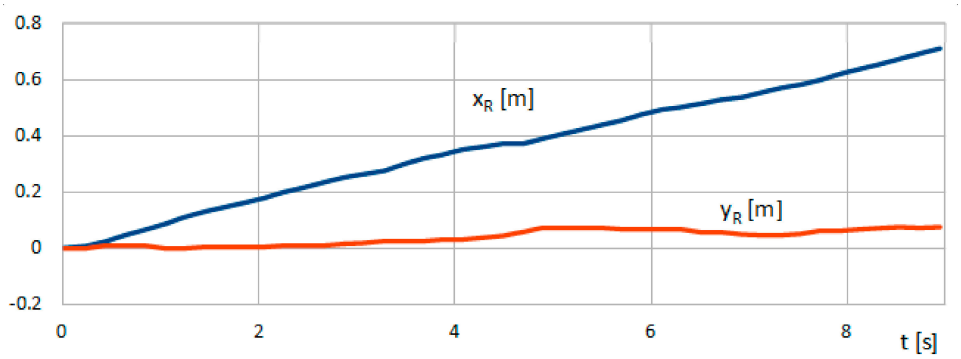

Figure 33. Plots of coordinates x_R, y_R of point *R on the robot's body* during the ride along the transverse axis with correction.

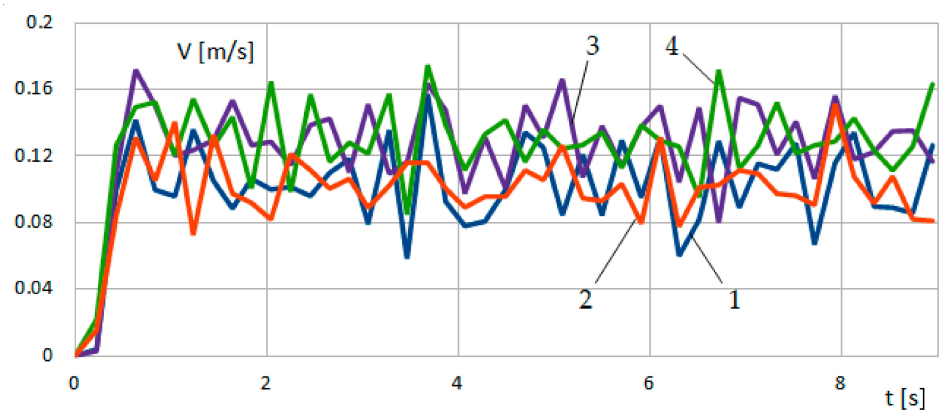

Figure 34. Waveforms of real linear speeds v_1, v_2, v_3, v_4 of tracks *1, 2, 3, 4* of the robot during the ride along the transverse axis with correction.

The measurements showed that the obtained linear speeds of the tracks v_{i} assume values close to the set speeds v_{Rx} and v_{Ry}, which were corrected by values v_{kw} and v_{kp}. The differences between real value v_{i} and set value v_{Rx} for the longitudinal motion were $\Delta v_i < 0.02$ m/s (Figure 30), disregarding the temporary error jump at the start-up. For the transverse motion, the same value was $\Delta v_{\mathrm{i}} < 0.04$ m/s (Figure 34). In this case, analogically as in the transverse motion without correction, no temporary error jump of speed at start-up was recorded. Therefore, the worsening ability to maintain the set speed v_{i} of the tracks in the transverse motion was observed, which was probably caused by the occurrence of low friction between the surface and the track.

Both in the case of the transverse and longitudinal motion, there was a significant flattening of the trajectory curve (Figures 27 and 31). In the presented case, the final change of orientation angle $\Delta\alpha$ of the body during longitudinal movement after the introduction of corrective speeds v_{kw} was 1.4° (Figure 28), while the final point R location error was $\Delta y_{\mathrm{R}} = 0.01$ m (Figure 29). A fourfold improvement of the drive parameter $\Delta\alpha$ was obtained (Table 2).

Table 2. Comparison of the conducted measurement results based on the distance of 0.7 m for the transverse motion, and 1.2 m for the longitudinal motion.

Longitudinal Motion		Transverse Motion	
Ride without Direction Correction	**Ride with Direction Correction**	**Ride without Direction Correction**	**Ride with Direction Correction**
$\Delta\alpha = 0.085$ rad $\Delta v_i < 0.02$ m/s $\omega_R = 0.009$ rad/s	$\Delta\alpha = 0.025$ rad $\Delta v_i < 0.02$ m/s $\omega_R = 0.003$ rad/s	$\Delta\alpha = 0.549$ rad $\Delta v_i < 0.03$ m/s $\omega_R = 0.052$ rad/s	$\Delta\alpha = 0.207$ rad $\Delta v_i < 0.04$ m/s $\omega_R = 0.024$ rad/s

In the case of transverse motion without speed correction, the robot did not cover the whole planned distance (Figure 25). Moreover, the measurement was stopped after covering 0.7 m at time $t = 9$ s (Figure 33), because the robot crossed the boundary of the measuring field in the direction of the Y axis. The same part of the trajectory was taken into account when analysing lateral movement while both considering and not considering, the correction of the driving (Figure 33).

The change of body orientation $\Delta\alpha$ after $t = 9$ s, i.e., at the time equal to the longitudinal drive without speed correction was 11° (Figure 32), while the location error was $\Delta y_{\mathrm{R}} = 0.07$ m (Figure 33).

In the transverse motion, the observed improvement trajectory curve was smaller than in the case for longitudinal motion. This resulted from, among other things, a 50% decrease in the required corrective speed v_{kp}, which took place for equipment-related reasons. The so-reduced correction is not perfectly efficient and therefore it did not allow for the complete improvement of the robot's trajectory. The obtained improvement (over a threefold reduction of error $\Delta\alpha$ (Table 2)), however, proved the correctness of the used method in the transverse motion of the robot.

The obtained measurement results of drive parameters were statistically analysed and are presented in Table 2.

4. Discussion

The paper presents a solution for a robot equipped with completely overlapping multidirectional tracks with a symmetrical roller position. A light robot prototype was designed and constructed using additive manufacturing technology to be later used in experimental research on a specially constructed test measurement bench. The robot's parameters were examined along the longitudinal and transverse axes.

The experimental research without ride direction correction confirmed the occurrence of the effect of motion trajectory deviation during transverse motion. Similar effects of the trajectory curve were observed during the simulation tests of the robot with non-overlapping tracks [27] and with partly overlapping tracks [24].

The data quoted in the references indicate a 3.8% deviation between the theoretical speed and the one obtained in the dynamic simulation during transverse motion, and less than a 1% deviation in the main motion. In these references, no quantitative data was presented regarding the change in the angular orientation of the robot.

The data obtained during the conducted experiment showed a deviation increment of 0.016 rad/s in the longitudinal motion, and 0.133 rad/s in the transverse motion.

Such significant values of the trajectory curve probably result from the mechanical imperfections of the prototype, which were probably due to the adopted drive system's structure without idling rolls and the used manufacturing technology. The fact that the track links and rollers were made of TPU filament, were of 40D hardness in the Shor scale, and had a low friction coefficient resulted in low adhesion of the robot to the surface. It was shown that this effect could be corrected using a suitable control system. The proposed static method of ride direction correction performed this role. The application of the continuous track speed correction allowed the angular deviation during longitudinal motion to be reduced to 0.007 rad/s, and to 0.019 rad/s during transverse motion. Despite the used correction by a value smaller than would result from the transverse motion calculations, a significant improvement in trajectory parameters was observed. This confirms the correctness of the used method and creates opportunities for further research and experiments.

The downside of the used correction method is the fact that it is a static method, which means that it requires earlier experimental tests of a robot on a particular type of surface, with the results needing to be used as the basis for the determination of efficient correction parameters. The application of a dynamic method of ride direction correction would improve the performance even more, and, in effect, eliminate the consequences of deviations in trajectory during robot motion. In further research stages, the prototype will be equipped with additional body orientation angle measurement sensors, which will allow the use of dynamic motion direction correction.

5. Conclusions

The key considerations of this paper were the design and testing of a mobile robot with an omnidirectional track. The research confirmed the ability of the robot to drive omnidirectionally while maintaining a fixed body orientation. The use of multidirectional tracks in the construction of mobile robots significantly increases their manoeuvrability.

The obtained results clearly show that vehicles equipped with continuous track systems with multidirectional tracks can still be improved. The application of the approach, involving the compensation of mechanical imperfections with the use of additional sensors and appropriate control, will allow for an even more precise maintenance of the set motion direction. The mechanical design of the track system also had a great influence on the accuracy of the robot's movement. Introducing additional road wheels and idlers or changing the material and geometry of the rollers in the track links will improve the contact between the track and the ground.

The development of systems equipped with continuous track systems could be used, inter alia, in the construction of equipment operating on narrow construction sites with numerous obstacles. Tracked machines, which are able to move in the transverse direction, would facilitate manoeuvring and contribute to reducing the number of accidents. Another potential area of application is the transport of small, yet heavy loads, in very limited spaces—in this case a uniform load distribution on the whole track could be of key significance for the usability of such vehicles.

Author Contributions: Conceptualization, M.F. and J.B.; methodology, M.F. and J.B.; software, M.F.; validation, M.F. and J.B.; formal analysis, M.F. and J.B.; investigation, M.F. and J.B.; resources, M.F.; data curation, M.F. and J.B.; writing—original draft preparation, M.F.; writing—review and editing, M.F. and J.B.; visualization, M.F.; supervision, J.B.; project administration, M.F. and J.B.; funding acquisition, J.B. All authors have read and agreed to the published version of the manuscript.

Funding: This work was supported by Grants-in-Aid at Wroclaw University of Science and Technology, Faculty of Mechanical Engineering, Poland, (No. 8211104160).

Institutional Review Board Statement: Not applicable.

Informed Consent Statement: Not applicable.

Data Availability Statement: Contact via email.

Conflicts of Interest: The authors declare no conflict of interest.

References

1. Mobile Robots Market by Operating Environment (Aerial, Ground, and Marine), Component (Control System, Sensors), Type (Professional and Personal & Domestic Robots), Application (Domestic, Military, Logistics, Field), and Geography—Global Forecast 2023. Markets and Markets SE 3610. Available online: https://www.marketsandmarkets.com/Market-Reports/mobile-robots-market-43703276.html?gclid=CjwKCAiAksyNBhAPEiwAlDBeLNKlJXjxNs2XgzEZLhSGhCanirlhMDnTZn9YKn3O3mNjX-upD3xwBhoCD6wQAvD_BwE (accessed on 11 December 2021).
2. Irobot. Available online: https://irobot.pl/pl/outlet/312-irobot-roomba-980-5060359281043.html (accessed on 27 October 2020).
3. Husqvarna. Available online: https://www.husqvarna.com/pl/produkty/kosiarki-automatyczne (accessed on 27 October 2020).
4. Moreno, J.; Clotet, E.; Lupiañez, R.; Tresanchez, M.; Martínez, D.; Pallejà, T.; Casanovas, J.; Palacín, J. Design, Implementation and Validation of the Three-Wheel Holonomic Motion System of the Assistant Personal Robot (APR). *Sensors* **2016**, *16*, 1658. [CrossRef]
5. Wong, J.Y.; Huang, W. "Wheels vs. tracks"—A fundamental evaluation from the traction perspective. *J. Terramech.* **2006**, *43*, 27–42. [CrossRef]
6. Bałchanowski, J. Modelling and simulation studies on the mobile robot with self-leveling chassis. *J. Theor. Appl. Mech.* **2016**, *54*, 149–161. [CrossRef]
7. Sperzyński, P.; Bałchanowski, J.; Gronowicz, A. Simulation of motion of a mobile robot on uneven terrain. *J. Theor. Appl. Mech.* **2020**, *58*, 541–552. [CrossRef]
8. Gronowicz, A.; Szrek, J. Design of LegVan Wheel-Legged Robot'sMechanical and Control System. *SYROM* **2009**, 145–158.
9. Machado, J.A.T.; Silva, M.F. An Overview of Legged Robots. In Proceedings of the MME 2006—International Symposium on Mathematical Methods in Engineering, Ankara, Turkey, 27–29 April 2006.
10. Raibert, M.; Blankespoor, K.; Nelson, G.; Playter, R. BigDog, the Rough-Terrain Quadruped Robot. *IFAC Proc. Vol.* **2008**, *41*, 10822–10825. [CrossRef]
11. Bledt, G.; Powell, M.J.; Katz, B.; Di Carlo, J.; Wensing, P.M.; Kim, S. MIT Cheetah 3: Design and Control of a Robust, Dynamic Quadruped Robot. In Proceedings of the 2018 IEEE/RSJ International Conference on Intelligent Robots and Systems (IROS), Madrid, Spain, 1–5 October 2018; pp. 2245–2252.
12. Hornback, P. The Wheel Versus Track Dilemma. *ARMOR* **1998**, *26*, 33–34.
13. Hertig, L.; Schindler, D.; Bloesch, M.; Remy, C.D.; Siegwart, R. Unified state estimation for a ballbot. In Proceedings of the Robotics and Automation (ICRA), 2013 IEEE International Conference on Robotics and Automation, Karlsruhe, Germany, 6–10 May 2013.
14. Seeman, M.; Broxvall, M.; Saffiotti, A.; Wide, P. An Autonomous Spherical Robot for Security Tasks. In Proceedings of the Computational Intelligence for Homeland Security and Personal Safety, Alexandria, VA, USA, 16–17 October 2006.
15. Guardbot. Available online: https://guardbot.org/ (accessed on 27 October 2020).
16. Lee, Y.; Yoon, D.; Oh, J.; Kim, H.S.; Seo, T. Novel Angled Spoke-Based Mobile Robot Design for Agile Locomotion with Obstacle-Overcoming Capability. *IEEE/ASME Trans. Mechatron.* **2020**, *25*, 1980–1989. [CrossRef]
17. Romano, D.; Donati, E.; Benelli, G.; Stefanini, C. A review on animal–robot interaction: From bio-hybrid organisms to mixed societies. *Biol. Cybern.* **2019**, *113*, 201–225. [CrossRef] [PubMed]
18. Ilon, B.E. Wheels for a Course Stable Selfpropelling Vehicle Movable in Any Desired Direction on the Ground or Some Other Base. U.S. Patent US3876255A, 8 April 1975.
19. Li, Y.; Ge, S.; Dai, S.; Zhao, L.; Yan, X.; Zheng, Y.; Shi, Y. Kinematic Modeling of a Combined System of Multiple Mecanum-Wheeled Robots with Velocity Compensation. *Sensors* **2019**, *20*, 75. [CrossRef] [PubMed]
20. Palacín, J.; Martínez, D.; Rubies, E.; Clotet, E. Suboptimal Omnidirectional Wheel Design and Implementation. *Sensors* **2021**, *21*, 865. [CrossRef]
21. Imetron GmbH. Mecanum Wheel. Attribution-ShareAlike 3.0 Unported (CC BY-SA 3.0). Available online: https://de.wikipedia.org/wiki/Mecanum-Rad#/media/Datei:Meacnum-Rad.png (accessed on 27 October 2020).
22. Gwpcmu. Mecanum Wheel. Attribution 3.0 Unported (CC BY 3.0). Available online: https://en.wikipedia.org/wiki/Mecanum_wheel#/media/File:UranusOmniDirectionalRobotPodnar.png (accessed on 27 October 2020).
23. Wu, M.; Dai, S.-L.; Yang, C. Mixed Reality Enhanced User Interactive Path Planning for Omnidirectional Mobile Robot. *Appl. Sci.* **2020**, *10*, 1135. [CrossRef]
24. Palacin, J.; Rubies, E.; Clotet, E.; Martinez, D. Trajectory of a human-sized mobile robot using three omnidirectional wheels: From simulation to implementation. In press. *Sensors* **2021**, *21*, 7216.

25. Yamada, N.; Komura, H.; Endo, G.; Nabae, H.; Suzumor, K. Spiral Mecanum Wheel Achieving Omnidirectional Locomotion in Step-Climbing. In Proceedings of the 2017 IEEE International Conference on Advanced Intelligent Mechatronics (AIM), Munich, Germany, 3–7 July 2017; pp. 1285–1290.
26. Bae, J.-J.; Kang, N. Design Optimization of a Mecanum Wheel to Reduce Vertical Vibrations by the Consideration of Equivalent Stiffness. *Shock. Vib.* **2016**, *2016*, 5892784. [CrossRef]
27. Moreno, J.; Clotet, E.; Tresanchez, M.; Martínez, D.; Casanovas, J.; Palacín, J. Measurement of Vibrations in Two Tower-Typed Assistant Personal Robot Implementations with and without a Passive Suspension System. *Sensors* **2017**, *17*, 1122. [CrossRef]
28. Rizzo, C.; Lagraña, A.; Serrano, D. GEOMOVE: Detached AGVs for Cooperative Transportation of Large and Heavy Loads in the Aeronautic Industry. In Proceedings of the 2020 IEEE International Conference on Autonomous Robot Systems and Competitions (ICARSC), Ponta Delgada, Portugal, 15–17 April 2020; pp. 126–133.
29. Mortensen Ernits, R.; Hoppe, N.; Kuznetsov, I.; Uriarte, C.; Freitag, M. A New Omnidirectional Track Drive System for Off-Road Vehicles. In Proceedings of the XXII International Conference on "Material Handling, Constructions and Logistics", Belgrade, Serbia, 4–6 October 2017.
30. Isoda, T. Roller-Crawler Type of Omni-Directional Mobile Robor for Off-Road Running. *IEEE Trans. Robot. Autom.* **2002**, *18*, 251–256.
31. Zhang, Y.; Huang, T. Research on a tracked omnidirectional and cross-country vehicle. *Mech. Mach. Theory* **2015**, *87*, 18–44. [CrossRef]
32. Zhang, Y.; Yang, H.; Fang, Y. Design and motion analysis of a novel track platform. *J. Phys. Conf. Ser.* **2018**, *1074*, 012014. [CrossRef]
33. Fang, Y.; Zhang, Y.; Li, N.; Shang, Y. Research on a medium-tracked omni-vehicle. *Mech. Sci.* **2020**, *11*, 137–152. [CrossRef]
34. Tao, H.; Yunan, Z.; Peng, T.; Nanming, Y.; Jian, Z. Design & Kinematics Analysis of a Tracked OmnidirectionalMobile Platform. *J. Mech. Eng.* **2014**, *50*, 206–212.
35. Guillén Ruiz, S.; Calderita, L.V.; Hidalgo-Paniagua, A.; Bandera Rubio, J.P. Measuring Smoothness as a Factor for Efficient and Socially Accepted Robot Motion. *Sensors* **2020**, *20*, 6822. [CrossRef] [PubMed]
36. Lin, H.-Y.; He, C.-H. Mobile Robot Self-Localization Using Omnidirectional Vision with Feature Matching from Real and Virtual Spaces. *Appl. Sci.* **2021**, *11*, 3360. [CrossRef]
37. OpenCV. Available online: https://opencv.org/ (accessed on 13 May 2021).